



ELSEVIER

Contents lists available at www.sciencedirect.com

Journal of Molecular Biology

journal homepage: <http://ees.elsevier.com/jmb>

Elucidating Substrate and Inhibitor Binding Sites on the Surface of GSK-3 β and the Refinement of a Competitive Inhibitor

Avital Licht-Murava¹, Batya Plotkin¹, Miriam Eisenstein²
and Hagit Eldar-Finkelman^{1*}

¹Department of Human Molecular Genetics and Biochemistry, Sackler School of Medicine, Tel Aviv University, Tel Aviv 69978, Israel

²Department of Chemical Research Support, Weizmann Institute of Science, Rehovot 76100, Israel

Received 8 December 2010;
received in revised form
7 February 2011;
accepted 16 February 2011
Available online
25 February 2011

Edited by M. Guss

Keywords:

protein kinase;
molecular modeling;
structure/function;
inhibitors;
drug design;
parasite GSK-3

A molecular understanding of substrate recognition of protein kinases provides an important basis for the development of substrate competitive inhibitors. Here, we explored substrate recognition and competitive inhibition of glycogen synthase kinase (GSK)-3 β using molecular and computational tools. In previous work, we described Gln89 and Asn95 within GSK-3 β as important substrates binding sites. Here, we show that the cavity bordered by loop 89-QDKRFKN-95, located in the vicinity of the GSK-3 β catalytic core, is a promiscuous substrate binding subsite. Mutations within this segment highlighted Phe93 as an additional essential contact residue for substrates' recognition. However, unlike Gln89 and Asn95, Phe93 was also important for the binding of our previously described substrate competitive inhibitor, L803 [KEAPPAPPQS(p)P], and its cell-permeable variant L803-mts. The effects of the substitution of charged or polar residues within L803 further suggested that binding to GSK-3 β is governed by hydrophobic interactions. Our computational model of GSK-3 β bound to L803 was in agreement with the experimental data. It revealed L803 binding with a hydrophobic surface patch and identified interactions between Pro8 (L803) and Phe93 (GSK-3 β). Computational modeling of new L803 variants predicted that inhibition would be strengthened by adding contacts with Phe93 or by increasing the hydrophobic content of the peptide. Indeed, the newly designed L803 variants showed improved inhibition. Our study identified different and overlapping elements in GSK-3 β substrate and inhibitor recognition and provides a novel example for model-based rational design of substrate competitive inhibitors for GSK-3.

© 2011 Elsevier Ltd. All rights reserved.

*Corresponding author. E-mail address:

heldar@post.tau.ac.il.

Abbreviations used: GSK, glycogen synthase kinase; HEK, human embryonic kidney; WT, wild type; IRS-1, insulin receptor substrate-1; CREB, cAMP-responsive element binding protein; MD, molecular dynamics; SEM, standard error of the mean.

Introduction

Protein kinases and phosphorylation cascades are essential for life, and they play key roles in the regulation of many cellular processes including cell proliferation, cell cycle progression, metabolic homeostasis, transcriptional activation and development.^{1–4} Aberrant regulation of protein phosphorylation underlies many human

diseases,^{2,3,5,6} and this has prompted the development and the design of protein kinase inhibitors.⁵⁻⁹ Most of the protein kinase inhibitors developed so far compete with ATP for its binding site. These inhibitors, although often very effective, generally show limited specificity¹⁰ due to the fact that the ATP binding site is highly conserved among protein kinases. Other sites, such as the substrate's binding site, show more variability in their shape and amino acid composition and may serve as favorable sites for drug design.¹¹ The understanding of substrate recognition and specificity is essential for the development of substrate competitive inhibitors. This knowledge, however, is limited by the scarce amount of structural data regarding substrate binding.

Glycogen synthase kinase (GSK)-3 is a constitutively active serine/threonine kinase that modulates diverse cellular functions including metabolism, cell survival and migration, neuronal signaling and embryonic development.¹²⁻¹⁶ Deregulation of GSK-3 activity has been implicated in the pathogenesis of human diseases such as type 2 diabetes and certain neurodegenerative and psychiatric disorders.¹⁷⁻²² Selective inhibition of GSK-3 is thought to be of therapeutic value in treating these disorders.²²⁻²⁶ Understanding of how GSK-3 interacts with its substrates may pave the way for the design and development of new substrate competitive GSK-3 inhibitors.

In a previous study, we reported the development of a novel class of substrate competitive inhibitors for GSK-3.²⁷ Our initial design was based on the unique substrate recognition motif of GSK-3 that includes a phosphorylated residue (usually serine) in the context of SXXXS(p) (where S is the target serine, S(p) is phosphorylated serine and X is any amino acid).^{28,29}

Structural studies on GSK-3 β identified a likely docking site for the phosphorylated residue; it is a positively charged binding pocket composed of Arg96, Arg180 and Lys205.^{30,31} Short phosphorylated peptides patterned after the GSK-3 substrates behaved as substrate competitive inhibitors.²⁷ The L803 peptide KEAPPAPPQS(p)P derived from the substrate heat shock factor-1³² was the best inhibitor of those evaluated.²⁷ An advanced version of L803, the cell-permeable peptide L803-mts,²⁷ was shown to promote beneficial biological activities under conditions associated with diabetes, neuron growth and survival and mood behavior.³³⁻³⁸

Focusing on substrate recognition of GSK-3, we identified three positions in the vicinity of the catalytic site (F67 in the P-loop, Q89 and N95) that were important for GSK-3 substrates binding.³⁹ Here, we looked for a common denominator in the substrate and in L803 binding sites. We show that the 89-QDKRFKN-95 segment defines a binding subsite for diverse GSK-3 substrates and contributes to L803 binding. Based on these observations and on a model of the GSK-3 β /ATP-Mg²⁺/L803 complex, we design improved inhibitors.

Results and Discussion

The Q89–N95 segment defines a substrate binding subsite

The sequence segment delimited by Gln89 and Asn95, two residues that are critical in GSK-3 substrate binding,³⁹ forms a loop (termed here the 89–95 loop) that, together with the conserved P-loop,

Fig. 1. The 89–95 loop defines a substrate binding subsite for GSK-3 β . (a) Features of the substrate binding site of GSK-3 β . The structure of GSK-3 β is based on the available crystal structures,^{30,40} as described in Ref. 39. The surface of GSK-3 β is shown in gray, with the loop 89–95 shown in yellow [its sequence is given in (b)] and the P-loop residue Phe67 emphasized in green. The positive ends of the residues that form the putative PO₃²⁻ binding cavity are indicated in blue. The ATP molecule is colored by atom type, with the Mg²⁺ ion colored black. Note that Q89, N95 and F93 form the bottom and a “wall” of a surface cavity located between the 89–95 loop and the P-loop. This cavity, which is highlighted in the inset, is a potential substrate binding subsite that can accommodate a variety of amino acid side chains. The predicted positions of Arg (dark blue), Lys (blue), His (cyan), Gln (magenta), Leu (green), Met (orange), Phe (black), Trp (purple) and Tyr (red) bound to the cavity are shown. The C β atoms of these side chains are shown as spheres. The predictions were obtained by computational anchoring spots mapping of the individual amino acids.⁴¹ (b) Sequence of the Q89–N95 loop and respective mutations generated within this segment. (c) Expression of GSK-3 β mutants. HEK-293 cells were transiently transfected with cDNA constructs expressing WT GSK-3 β , D90A, K91A, R92A, F93A and R94A mutant proteins, as described in **Materials and Methods**. Cell extracts were subjected to Western blot analysis using either anti-GSK-3 β or anti-phospho-GSK-3 (Tyr216/Tyr274 for α or β isoforms, respectively) antibodies. The control (c) represents extracts from cells expressing the empty vector. (d) Phosphorylation of peptide substrates by F93A mutant. F93A was subjected to *in vitro* kinase assays with substrates pIRS-1, p9CREB and PGS-1 as described in **Materials and Methods**. The percentage of substrate phosphorylation obtained with WT GSK-3 β , which was defined as 100%, and the results are means of two to three independent experiments, each performed in duplicates \pm standard error of the mean (SEM). (e) Phosphorylation of substrate proteins by F93A in cells. HEK-293 cells were co-transfected with WT GSK-3 β or F93A plasmids together with construct coding for CREB. Cells were treated with forskolin (10 μ M, 1 h), and cell extracts were subjected to Western blot analysis using anti-phospho-CREB (Ser129/Ser133) antibody. Expression levels of CREB and GSK-3 proteins are indicated. (f) The same as (d), except that N'IRS-1 cDNA construct was used instead of CREB, and cells were treated with phorbol ester (100 nM, 30 min). Anti-phospho-IRS-1 (Ser332) antibody was used as indicated. Expression levels of N'IRS-1 and GSK-3 β are indicated. The ratio of pCREB/CREB or of pN'IRS-1/N'IRS-1 as calculated from densitometry analysis is shown on the right panel of each figure. Results are means of three independent experiments \pm SEM.

defines the borders of a surface cavity (Fig. 1a). Gln89 and Asn95 point toward the cavity, indicating that it is a likely substrate binding subsite (Fig. 1a). Using the recently developed anchoring spots mapping procedure,⁴¹ we found that a variety of amino acid side chains can make favorable contacts within this cavity (Fig. 1a), suggesting that the subsite is promiscuous, in line with the variability of GSK-3 substrates. To further explore the role of the 89–95 loop in GSK-3 β substrate binding, each of the amino acid residues within this segment was individually mutated to alanine (see Fig. 1b). The generated mutants (D90A, K91A, R92A, F93A and K94A) were transiently expressed in human embryonic kidney (HEK)-293 cells. All the mutants were expressed at levels considerably above that of the endogenous GSK-3 β (Fig. 1c, upper panel). Similar to the wild-

type (WT) GSK-3 β , the mutants were phosphorylated at Tyr216 (Fig. 1c, lower panel), indicating that their catalytic activity was not impaired by the mutation, as phosphorylation at Tyr216 reflects an auto-phosphorylation process.^{42,43}

The GSK-3 β mutants were partially purified by ion-exchange chromatography, and their abilities to phosphorylate peptide substrates were tested in *in vitro* kinase assays. The substrates were pIRS-1, p9CREB and pGS-1, which are phosphorylated peptides derived from the insulin receptor substrate-1 (IRS-1),⁴⁴ cAMP-responsive element binding protein (CREB)³⁹ and glycogen synthase,³⁹ respectively. Three of the five mutants, R92A, F93A and K94A mutants, impaired the ability to phosphorylate the substrates (Table 1). Mutation at Lys91 enhanced substrate phosphorylation by about

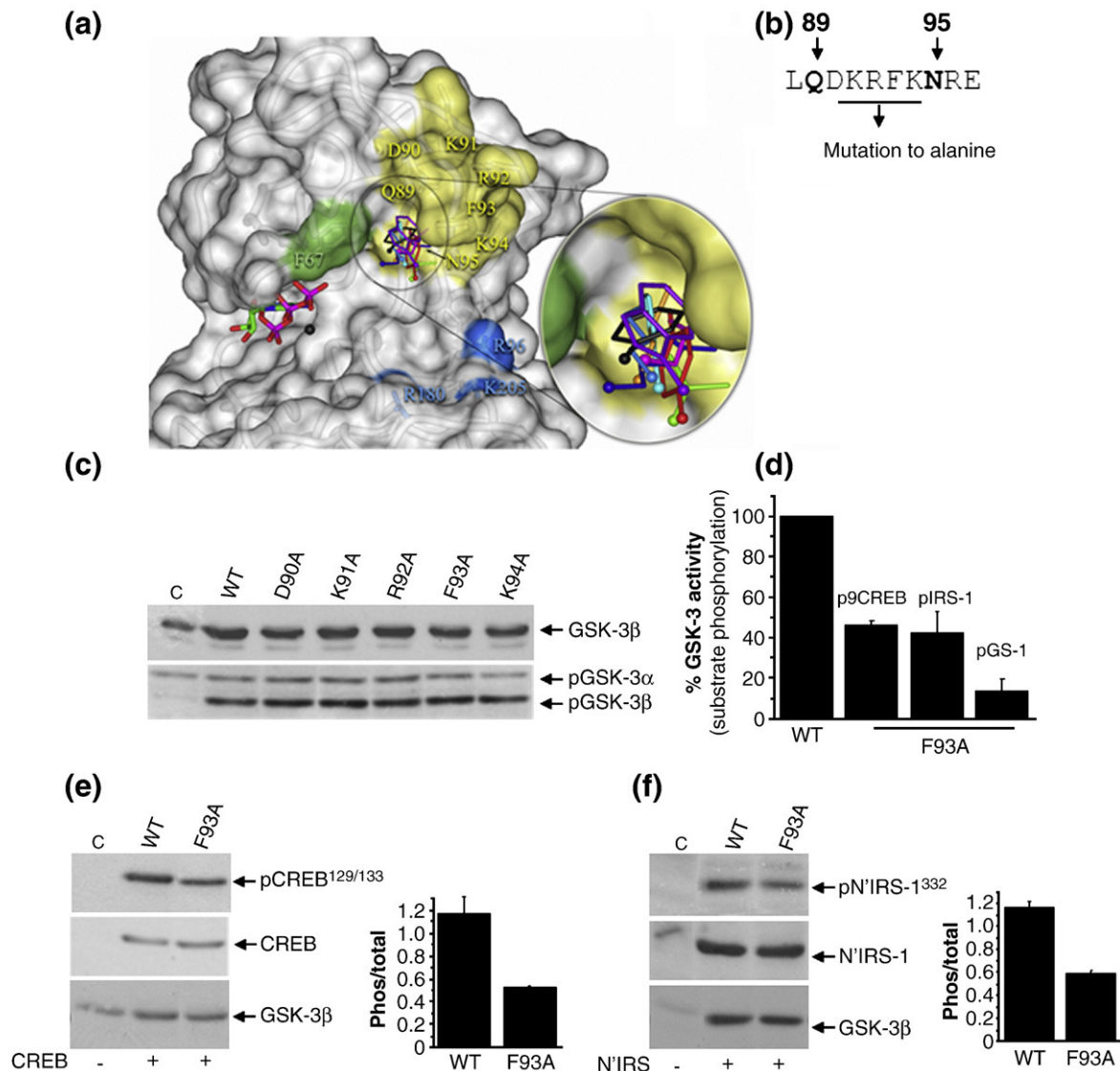


Fig. 1 (legend on previous page)

Table 1. Phosphorylation of GSK-3 substrates by various mutants

Mutant	pIRS-1	p9CREB	pGS-1
D90A	88±15	92±21	83±2
K91A	140±18	161±5	119±5
R92A	60±3	49±19	41±14
F93A	42±13	46±2	13±7
K94A	52±19	71±4	19±14

The results present the percentage of substrate phosphorylation (indicated peptides are pIRS-1, p9CREB and pGS-1) obtained with WT GSK-3 β , which was set to 100%, and are means of two to three independent experiments, each performed in duplicates \pm SEM.

20–60% (Table 1). Notably, mutation at Phe93 had the most deleterious effect for all substrates, reducing the kinase ability to phosphorylate them by more than 50% (Table 1 and Fig. 1d). A similar impact was observed with Q89A and N95A mutants.³⁹ Hence, Phe93 adjoins Gln89 and Asn95 as an important substrate binding position. Phe93 located within the 89–95 loop, is highly exposed (81% solvent accessibility) and faces the substrate binding cavity, facilitating contacts with a variety of residues. We next verified the role of Phe93 in substrate binding by employing a cellular system and protein substrates (i.e., not peptides). To this end, the WT GSK-3 β and F93A mutant were expressed in HEK-293 cells together with GSK-3 substrates CREB or N'IRS-1 (the N-terminal region of IRS-1⁴⁴). Because GSK-3 requires pre-phosphor-

ylation of its substrates, we treated the cells with forskolin to enhance CREB phosphorylation via activation of cAMP-dependent kinase (protein kinase A)⁴⁵ or with phorbol ester to enhance N'IRS-1 phosphorylation via activation of protein kinase C⁴⁶ (see Fig. 1S). We then examined the phosphorylation of CREB at serine 129 and the phosphorylation of N'IRS-1 at serine 332 (both GSK-3 phosphorylation sites). Unlike WT GSK-3 β , the expression of F93A did not enhance the phosphorylation of these substrates as determined by specific anti-phospho-antibodies (Fig. 1e and f). This substantiated the *in vitro* results showing that Phe93 interacts with GSK-3 substrates under cellular conditions.

The 89–95 loop is not conserved in unicellular organisms

The 89–95 loop is highly conserved in the vertebrate kingdom³⁹ (and unpublished results from our laboratory), but some variability is found in the lower unicellular organisms choanoflagellate and apicomplexa (Fig. 2a). In choanoflagellate, Lys91 is replaced by arginine, and Phe93 is replaced by tyrosine. In *Plasmodium falciparum* (the parasite causing malaria), the three consecutive amino acids corresponding to positions 91–93 are replaced by proline, glutamine and tyrosine (Fig. 2a). In *Trypanosoma brucei* (*T. brucei*) GSK-3 short, Lys91 and Phe93 are replaced by proline and tyrosine, respectively. Interestingly, in *T. brucei* GSK-3 long, none of the loop residues match the vertebrate consensus (Fig. 2a). Indeed, this GSK-3 form showed distinct

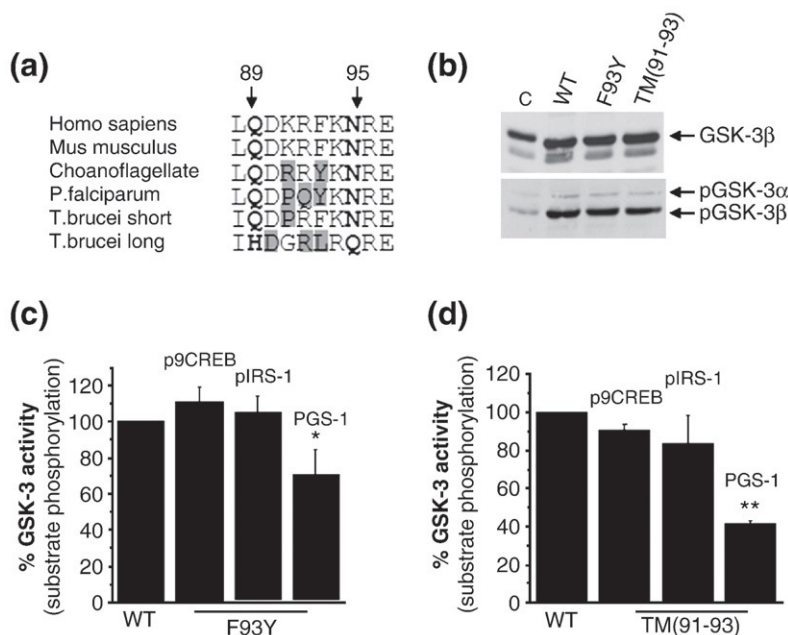


Fig. 2. Natural “mutations” at the 89–95 loop and their impacts on GSK-3 substrate recognition. (a) Alignment of the Q89–N95 sequence of GSK-3 β from non-vertebrate species in which this loop is not conserved. The different residues are marked gray. (b) Expressions of F93Y and TM 91–93 mutants in HEK-293 cells and levels of phosphorylation at Tyr216. (c) Substrate phosphorylation by F93Y. WT GSK-3 β and F93Y mutant were subjected to *in vitro* kinase assays with pIRS-1, p9CREB and PGS-1 peptide substrates as described in Materials and Methods. The percentage of substrate phosphorylation obtained with WT GSK-3 β was defined as 100%, and the results are

means of two independent experiments, each performed in duplicate. (d) The same as (c), except that TM (91–93) mutant was used. * $p < 0.05$; ** $p < 0.01$.

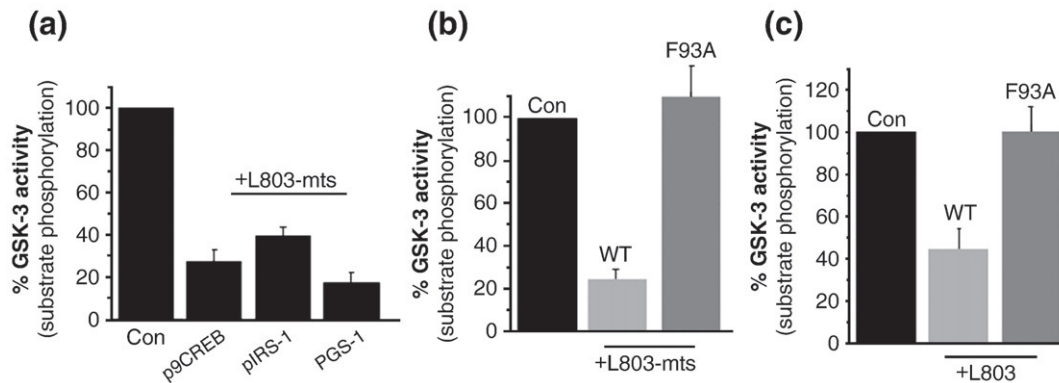


Fig. 3. Inhibition of GSK-3 β by L803 and L803-mts requires GSK-3-Phe93. (a) L803-mts competes with substrates. Purified GSK-3 β was subjected to *in vitro* kinase assays using pIRS-1, p9CREB and pGS-1 substrates in the presence or in the absence of L803-mts (100 μ M). (b) L803-mts does not inhibit substrate phosphorylation by F93A. WT GSK-3 β and F93A were subjected to *in vitro* kinase assays together with L803-mts. In both bars, the results present the percentages of substrate phosphorylation obtained with the inhibitor *versus* those of phosphorylation without the inhibitor (Con, defined as 100%), and they are means of two to three independent experiments \pm SEM. (c) The same as (b), except that L803 (200 μ M) was used.

biological activity compared to *T. brucei* GSK-3 short.⁴⁷ We thus focused on the natural variability found in the organisms containing the 89–95 loop. A mutant in which Phe93 was replaced by tyrosine (F93Y), and a mutant that copied the 89–95 loop in *Plasmodium* (TM 91–93; a triple mutant in which positions 91, 92 and 93 were replaced by proline, glutamine and tyrosine, respectively) were generated. The mutants were expressed in cells and were able to phosphorylate at tyrosine 216 (Fig. 2b). The mutants were then subjected to phosphorylation assays. We found that the F93Y mutant did not affect the ability of GSK-3 to phosphorylate pIRS-1 and p9CREB substrates but slightly reduced phosphorylation of pGS1 (Fig. 2c). TM 91–93 showed a more significant reduction in the phosphorylation of pGS1 (Fig. 2d). These results indicated that these natural changes in the 89–95 loop had a moderate effect on GSK-3 substrate recognition and suggested that different substrates have different sets of interactions with the individual residues within the loop (as also seen in Table 1). In addition, the fact that mutation at Phe93 to alanine impaired GSK-3 substrate phosphorylation (Table 1 and Fig. 1d–f), but its replacement by tyrosine was not deleterious, indicated that these residues interact with GSK-3 substrates via their aromatic ring.

Phe93 is required for the inhibition of GSK-3 by the substrate competitive inhibitors L803 and L803-mts

L803 is a selective substrate competitive inhibitor of GSK-3.²⁷ We performed the experiments with L803 or with its biologically active version L803-mts²⁷ (in which a myristic acid is attached to its N-terminus). L803-mts competes with various substrates (Fig. 3a),

indicating that its binding mode with GSK-3 may share interactions similar to those of GSK-3 substrates. Thus, we examined if L803-mts (or L803) interacts with the 89–95 loop. *In vitro* kinase assays were performed with WT GSK-3 β and GSK-3 β mutants in the presence or in the absence of the peptide inhibitors. Results indicated that L803-mts or L803 did not inhibit F93A (Fig. 3b and c). In contrast, all the other mutants including Q89A, N95A, R92A, K94A, F93Y and TM (91–93) were inhibited (not shown). Collectively, our results suggest that both inhibitors (L803 and L803-mts) and the substrates interact with Phe93; however, unlike the substrates, L803/L803-mts do not interact with other residues within the 89–95 loop including Gln89 and Asn95.

L803 binding with GSK-3 β is controlled by hydrophobic interactions

In view of the fact that Gln89 and Asn95 did not contribute to the binding of L803, we examined whether the binding involves any hydrophilic interactions. L803 includes two charged amino acids, Lys1 and Glu2, and a polar residue, Gln9 (Fig. 4a). New peptide variants were synthesized in which each of these residues was individually replaced by alanine (PK1A, PE2A and PQ9A peptides, respectively; Fig. 4a). The ability of each peptide to inhibit GSK-3 β was then determined by *in vitro* kinase assays as described previously. PK1A inhibited WT GSK-3 β to a similar extent as L803, but inhibition by PE2A was slightly impaired (Fig. 4b). In contrast, the inhibition by PQ9A, a peptide in which Gln9 was replaced by alanine, was stronger by about twofold relative to the inhibition by L803 (Fig. 4b). To further understand the contribution of position 9 to L803 function, we replaced Gln9 with

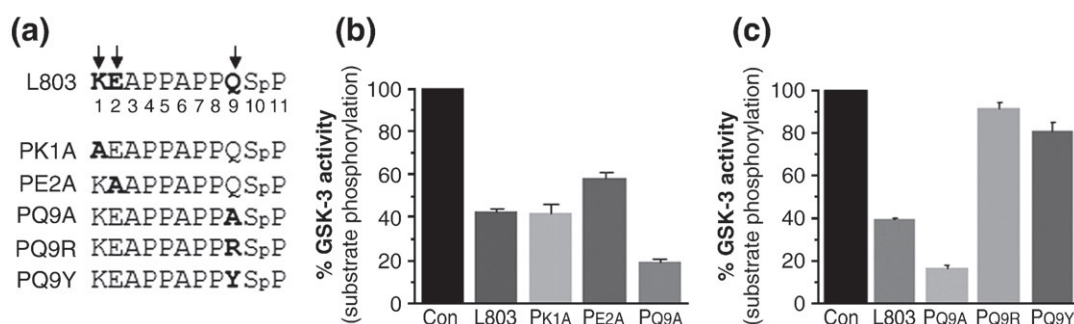


Fig. 4. L803 inhibition of GSK-3 does not involve hydrophilic interactions other than the interaction through S(p). (a) L803 variants used in this study. The positions that were changed to alanine and the substitution at position 9 are in boldface. Sp, phosphorylated serine. (b) The ability of L803 variants (250 μ M each) to inhibit GSK-3 β was determined by *in vitro* kinase assays as described in [Materials and Methods](#). Substrate phosphorylation obtained in reaction with no inhibitor that was defined as 100% (Con), and results presented are means of two independent experiments, each performed in duplicate \pm SEM. (c) The same as in (b), expect that L803 variants PQ9A, PQ9R and PQ9Y were used.

either the charged amino acid arginine (PQ9R) or the aromatic residue phenylalanine (PQ9F). Both replacements produced non-inhibitory L803 variants (Fig. 4c). It appears that the binding of L803 to GSK-3 β is mostly mediated by hydrophobic interactions and that a small amino acid in position 9 might be advantageous.

Modeling GSK-3 β interactions with the inhibitor

Predicting the binding modes of peptides is generally a difficult problem due to their inherent flexibility, which contributes to the high entropy of unbound peptides. This entropy barrier has to be overcome upon binding. However, in our study, the inhibitory peptide is proline rich, making it rather rigid. Molecular dynamics (MD) simulation of L803 in water, starting from a preliminary model of the peptide obtained by short energy minimization, showed that the free L803 adopts a polyproline-like helix for part of its structure. The conformers of L803 in the last 0.5 ns of the MD simulation were superposed and clustered by calculating the root-mean-square difference (RMSD) for all non-hydrogen atoms. The clustering produced four groups in which the RMSD between conformers within the group is below 3 \AA (Fig. 2S). The central conformer from each group was used in rigid-body docking.

Rigid-body docking of the L803 conformers to GSK-3 β was executed with the geometric–electrostatic–hydrophobic version of MolFit⁴⁸ followed by filtering based on statistical propensity measures and solvation energy estimates.⁴⁹ At this point, we introduced the requirement that S10(p) of L803 must reside near the phosphate binding cavity of GSK-3 β and found that only the search that employed the central L803 conformer from the largest MD group produced a high-ranking cluster of acceptable docking models. Docking of the central conformers

from the three other MD groups did not produce a plausible model.

MolFit allows for moderate conformational flexibility of side chains,⁵⁰ and to explore its sensitivity to the exact conformation of the peptide, we selected four additional conformers from the largest MD group that represent the range of structures within this group (Fig. 2S) and docked them to GSK-3 β . At least one acceptable docking model [in which S10(p) is in contact with the positive cavity of GSK-3 β] was obtained for three of these conformers; for the fourth conformer, we obtained an acceptable models when the docking scan was biased by up-weighting contacts through S10(p).⁵¹ These results indicated that RMSD of ~ 3 \AA for the peptide that do not involve large changes in the backbone are mostly tolerated by MolFit. Moreover, in this case, the rigid-body docking distinguished between the four MD groups, producing acceptable interaction models only for the largest MD group. The docking of five conformers from this group produced eight docking models, which form two subgroups that show slightly different orientations of the peptide and that differ in the conformation of L803 Pro11 (Fig. 5a). In all of the eight docking models, L803 is positioned in the deep groove near the P-loop (Fig. 3S), and it interacts with Phe93 through Pro8. In addition, L803 Pro5 interacts with a hydrophobic surface patch of GSK-3 β , which consists of Val214, the aromatic ring of Tyr216 and Ile217. In the smaller subgroup of docking models, an additional contact with GSK-3 β Phe93 is observed via L803 Pro11.

To further substantiate the rigid-body docking model, we performed a 2-ns MD simulation of the GSK-3 β /ATP–Mg²⁺/L803 complex in water. The starting structure of the complex consisted of GSK-3 β in complex with ATP and Mg²⁺ and the preliminary model of L803. L803 was positioned ~ 5 \AA away from the molecular surface of GSK-3 β , near the deep groove and with S10(p) opposite the

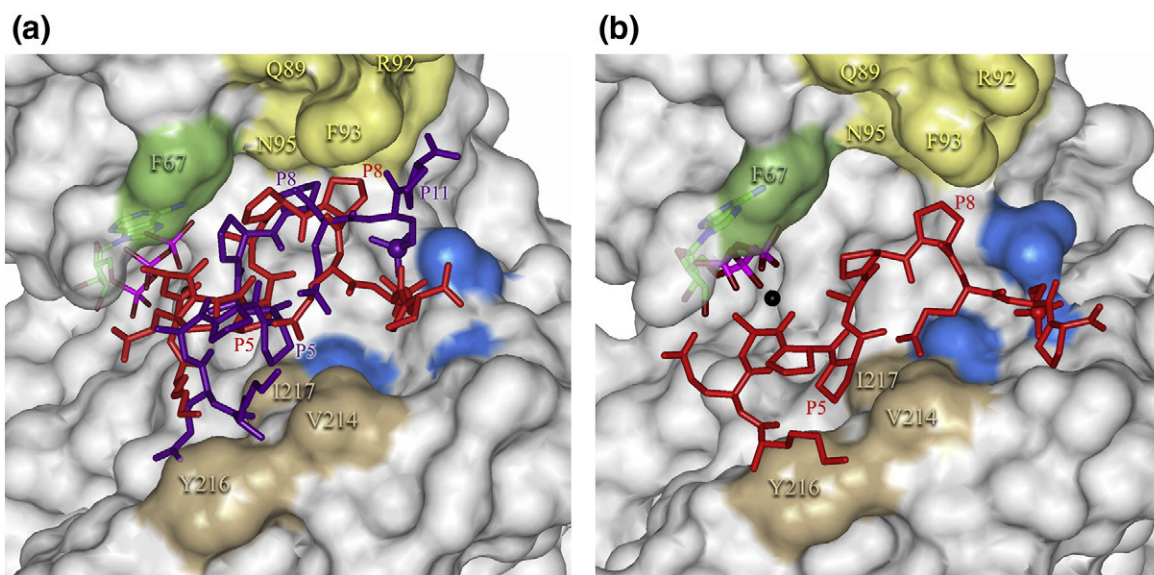


Fig. 5. Models for L803 binding with GSK-3 β . (a) Representative L803 poses from the two clusters obtained in the rigid-body docking (red for the large cluster and violet for the small cluster). (b) Representative model from the largest cluster in the MD simulation. The interactions of L803 with GSK-3 β in all the models consist of a charged interaction between S10(p) of L803 (whose phosphorous atom is indicated by a sphere) and the positive phosphate binding pocket of GSK-3 β (indicated blue) and of hydrophobic interactions between L803/P8 and GSK-3 β /F93 and between L803/P5 and a hydrophobic patch on the surface of GSK-3 β , indicated in beige.

positive phosphate binding site. The last 1 ns of the trajectory was clustered, and Fig. 5b presents a representative snapshot from the largest group, reflecting the most abundant binding mode. Notably, the peptide adopts a conformation very similar to that of the free peptide. Thus, the RMSD between the central model of free L803 in the largest MD group and the bound L803 is only 1.7 Å for all non-hydrogen atoms (Fig. 2S). It however moves away from the starting position and interacts with GSK-3 β in a manner similar to that observed in the rigid-body docking models. Thus, L803 Pro5 interacts with the hydrophobic surface patch of GSK-3 β (Val214, Ile217 and Tyr216), and Pro8 interacts with GSK-3 β Phe93. Ala6 of L803, located at the phosphorylation site, is found ~10 Å away from the ATP γ -phosphate, too far for phosphorylation. In line with the experimental results (Figs. 3 and 4), Phe93 of GSK-3 β interacts with Pro8 of L803, Gln89 and Asn95 of GSK-3 β are not involved in L803 binding and the charged residues of the peptide are solvent exposed. Gln9 of L803 is near GSK-3 β residue Val214 and contacts it in parts of the trajectory, yet in every case, the polar end of its side chain is exposed. A small hydrophobic residue, such as Ala, in this position can make the same interactions but is not entropically restricted, contributing to the better inhibition by PQ9A (Fig. 4b).

Our previous study on the interaction between pCREB and GSK-3 β suggested that the two helical segments of the substrate bind in the deep groove next to the P-loop and in a shallower groove near

Phe93³⁹ (Fig. 3S). The rigid-body docking did not detect binding of L803 in the shallow groove, but the experimental results do not rule out such binding. We therefore repeated the MD simulation with L803 near the shallow groove as a starting position. The most abundant structure in the last 1 ns of the simulation shows hydrophilic interactions between the charged residues of the peptide and the GSK-3 β ; Phe93 in this model makes no contact with the inhibitor (Fig. 3S). This result refutes the alternative binding mode of L803 in the shallow groove of GSK-3 β .

Designing improved inhibitors

The L803 binding model shows contacts between GSK-3 Phe93 and Pro8 and, possibly, Pro11 of L803 (Fig. 5). Additional contacts with Phe93 may improve the inhibition; therefore, MD simulations with the variant L803F, in which a Phe residue was added at the C-terminus, were performed. The results show that L803F has a conformation very similar to that of L803 (RMSD of 2.4 Å for the non-hydrogen atoms of the common residues; Fig. 2S), and it interacts extensively with Phe93, via its Pro8 and Phe12, and with the hydrophobic surface patch of GSK-3 β (Fig. 6a). We next performed *in vitro* kinase assays, which showed that the new peptide, L803F, has improved inhibition ability by about 50% relatively to L803 (Fig. 6b). The role of Phe93 in binding L803F was then validated. We found that the ability of L803F to inhibit F93A mutant was

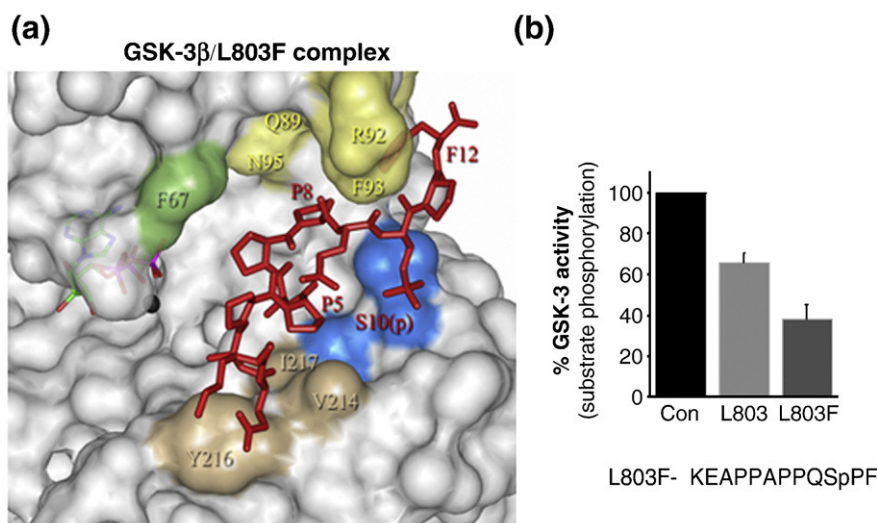


Fig. 6. The peptide inhibitor with strengthened contacts with Phe93 has improved efficacy. (a) Representative model from the largest cluster in the MD simulation showing the binding geometry of L803F. The peptide is slightly shifted toward GSK-3 β Phe93 and forms interactions with this residue. (b) Inhibition of GSK-3 β by L803F. *In vitro* kinase assays were performed with GSK-3 β in the presence of L803 or L803F (200 μ M each). Percentage of the substrate phosphorylation obtained without inhibitor was defined as 100% (Con), and results are means of two independent experiments \pm SEM.

significantly impaired, but to a smaller extent as compared with L803 (Fig. 4S and Fig. 3c). Thus, similar to L803, L803F interacts with Phe93, but the additional contacts with GSK-3 β (Fig. 6) enabled stronger interaction with F93A mutant.

Another variant of L803 was designed based on the experimental results for PQ9A (Fig. 4b). Assuming that the multiproline composition of L803 and its hydrophobic nature dominates the binding to GSK-3 β , we replaced Gln9 by proline, which is a small hydrophobic residue (PQ9P). Indeed, PQ9P inhibited GSK-3 β by \sim 80% more compared to L803 (Fig. 7a). MD simulation of free PQ9P in water showed that the peptide adopts a different conformation than L803. Also, clustering of the PQ9P MD conformers produced three groups and showed limited mobility within the largest group (Fig. 2S). Rigid-body docking of the central conformer from each MD group to GSK-3 β did not produce an acceptable interaction model in either the regular searches or the biased searches, in which contacts through S10(p) and the positive phosphate binding cavity of GSK-3 β were up-weighted. MD simulation of the GSK-3 β /ATP-Mg²⁺/PQ9P complex, starting with PQ9P near the deep groove and S10(p) opposite the positive phosphate binding groove, suggested that the bound PQ9P differs considerably from the free peptide (RMSD of 5.3 Å for the non-hydrogen atoms). The bound model of PQ9P was obtained in a short MD simulation that did not necessarily explore the whole conformational space; however, the proposed conformation change between bound and unbound PQ9P is corroborated by

the lack of suitable rigid-body docking models. Hence, the rigidity of this peptide does not help to lower the entropy barrier for binding. Our model suggests that the high affinity of PQ9P can be attributed to the extensive contacts with Phe93, Phe67 and additional contacts with the substrate binding cavity delimited by the P-loop and the 89–95 loop (Fig. 7b). PQ9P does not interact with the hydrophobic patch formed by V214, Y216 and I217. Hence, its general binding location differs from that of L803 and L803F (Figs. 5 and 6). Similar to L803, PQ9P's ability to inhibit F93A mutant was impaired though to a smaller extent as compared with L803 (Fig. 4S and Fig. 3c). Hence, PQ9P interacts with Phe93 (as predicted by our model); its stronger binding affinity to GSK-3 β (Fig. 7a) enabled a stronger interaction with F93A mutant.

The importance of the hydrophobic surface patch of GSK-3 β in binding peptide inhibitors

The hydrophobic surface patch that consists of Val214, the aromatic ring of Tyr216 and Ile217, was predicted to contribute to the binding of L803 and L803F (Figs. 5 and 6a) but not of PQ9P (Fig. 7b). We therefore tested the importance of this patch in binding these three peptide inhibitors. We generated a new mutant, V214A, in which Val214 was mutated to alanine. We chose to mutate Val214, since it makes multiple contacts with Pro5 (Figs. 5 and 6a) and is highly exposed (60% exposure). Ile217 is far less exposed (23%), and mutation of Tyr216 hampers the kinase function of GSK-3 β .⁵² We found that

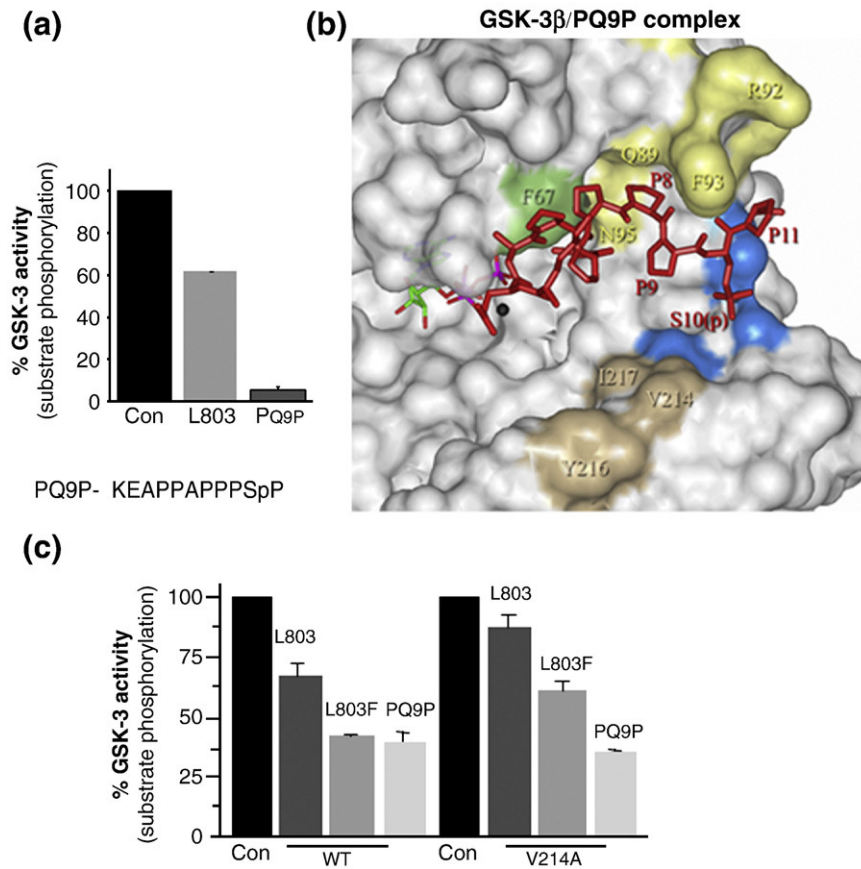


Fig. 7. The peptide inhibitor with Gln9 replaced with Pro9 has improved efficacy. (a) Inhibition of GSK-3 β by PQ9P. *In vitro* kinase assays were performed with GSK-3 β in the presence of L803 or PQ9P (200 μ M each). Substrate phosphorylation obtained without inhibitor was defined as 100%, and results are means of two independent experiments \pm SEM. (b) Representative model from the largest cluster in the MD simulation showing the binding geometry of PQ9P. (c) Role of Val214 in interacting with L803 and L803F. *In vitro* kinase assays were performed with WT GSK-3 β or V214A in the presence of L803, L803F (250 μ M each) and PQ9P (100 μ M), using pIRS-1 as a substrate. Results present the percentages of substrate phosphorylation obtained with the inhibitor *versus* those of phosphorylation obtained without the inhibitor (Con, defined as 100%) and are means of two independent experiments \pm SEM.

the ability of L803 and L803F to inhibit V214A was significantly impaired (Fig. 7c, about 20–25% reduction). On the other hand, PQ9P inhibition was not affected by this mutation (Fig. 7c). Taken together, these results support the existence of hydrophobic contacts between L803 and L803F, but not PQ9P, and GSK-3 β Val214.

In summary, the experimental and computational results presented here suggest that different yet partially overlapping surface regions of GSK-3 β are used for substrate and inhibitor binding, thus allowing for competitive inhibition. The substrate binds in the groove between the lobes and in a cavity bordered by the P-loop and the loop 89–95. It forms tight interactions with Gln89, Asn95³⁹ and Phe93 (in addition to its binding into the phosphate binding cavity previously described).^{30,31} Together, these surface features provide the correct environment for accurate positioning of the substrate,

which is essential for successful phosphorylation. The inhibitor, on the other hand, does not need exact positioning; its ability to bind to the positive phosphate binding cavity is essential for recognition, but it is not sufficient for high-affinity binding and efficient competitive inhibition. In the case of L803 inhibitor, its binding affinity is mediated by its hydrophobic interactions with Phe93 and the hydrophobic patch described here, together with its inherent rigidity that diminishes the entropic cost of binding and contributes to its binding affinity. This understanding led to the generation of the new inhibitor L803F that makes stronger contacts with Phe93. The even more potent inhibitor PQ9P has increased hydrophobic content and a different conformation compared to L803. It appears to bind in a somewhat different pose than L803 and L803F, near the P-loop and the substrate binding cavity. Our study thus provides

new prospects for the design of new substrate competitive inhibitors for GSK-3.

Materials and Methods

Materials

Peptides were synthesized by Genemed Synthesis, Inc. (San Francisco, CA, USA). The peptide substrates included p9CREB, ILSRRPS(p)YR; pIRS-1, RREGGMSRPAS(p)VDG; and PGS-1, YRRAAVPPSPSLSRHSSPSQS(p)EDEEE as previously described.³⁹ The peptide inhibitor L803 KEAP-PAPPQS(p)P and the L803-mts, in which myristic acid was attached to its N-terminus, were described previously.²⁷ Other L803 variants synthesized for this work are described in the text. Anti-GSK-3 β antibody was obtained from Transduction Laboratory (Lexington, KY, USA), anti-phospho-GSK-3 (Y²¹⁶) was obtained from Upstate Biotechnology (Lake Placid, NY, USA), anti-phospho-CREB (S^{129/133}) was obtained from BioSource International, Inc. (Camarillo, CA, USA), CREB antibody was obtained from Cell Signaling Technology (Beverly, MA, USA) and anti-phospho-IRS-1 (S³³²) was generated in our laboratory as described previously.⁴⁴ Radioactive materials were purchased from NEN PerkinElmer USA.

Plasmids and mutants

GSK-3 β in the pCMV4 vector⁴³ was used as the template for mutagenesis. Mutations were generated using Quik-Change Site-Directed Mutagenesis Kit (Stratagene, La Jolla, CA, USA) according to the manufacturer's protocols. Mutations included replacement of D90, K91, R92, F93 and K94 to alanine, replacement of F93 to tyrosine, and a triple mutation at residues 91–93. All constructs were sequenced to confirm the presence of desired mutations. The sequences of mutagenic oligonucleotides are available from the authors upon request. N'IRS-1 (also termed PTB2) plasmid was previously described.⁴⁴ The CREB-green fluorescent protein plasmid was purchased from Clontech (Mountain View, CA, USA).

Cell transfections and protein partial purifications

HEK-293 cells were grown in Dulbecco's modified Eagle's medium, supplemented with 10% fetal calf serum, 2 mM glutamine, 100 U/ml penicillin and 100 μ g/ml streptomycin. HEK-293 cells were transiently transfected with indicated constructs, using calcium phosphate method as described previously.³⁹ Cells were lysed in ice-cold buffer G [20 mM Tris-HCl (pH 7.5), 10 mM β -glycerophosphate, 10% glycerol, 1 mM ethylene glycol bis(β -aminoethyl ether) *N,N'*-tetraacetic acid, 1 mM ethylenediaminetetraacetic acid, 50 mM NaF, 5 mM sodium pyrophosphate, 0.5 mM orthovanadate, 1 mM benzamidine, 10 μ g/ml leupeptin, 5 μ g/ml aprotinin, 1 μ g/ml pepstatin and 0.5% Triton X-100]. Cell extracts were centrifuged at 15,000g for 30 min. Supernatants were collected, and equal amounts of proteins were boiled with SDS sample buffer, were subjected to gel electrophoresis (7.5–12% polyacrylamide gel), were transferred to nitro-

cellulose membranes and were immunoblotted with indicated antibodies. For partial purification, cells were lysed in buffer H [20 mM Tris (pH 7.3), 1 mM ethylene glycol bis(β -aminoethyl ether) *N,N'*-tetraacetic acid, 1 mM ethylenediaminetetraacetic acid, 1 mM orthovanadate, 25 μ g/ml leupeptin, 25 μ g/ml aprotinin, 25 μ g/ml pepstatin A, 500 nM microcystine LR and 0.25% Triton X-100]. The lysates were centrifuged at 15,000g. The resulting supernatants were passed through DE-52 minicolumns (Whatman, Maidstone, England) that were equilibrated with buffer H. GSK-3 β proteins were eluted with the same buffer containing 0.02 M NaCl. Equal amounts of proteins were used for *in vitro* kinase assays. In all experiments, GSK-3 mutants were expressed at levels at least fivefold higher than levels of the endogenous GSK-3 β as determined by Western blot analysis.

In vitro kinase assays

The GSK-3 β proteins (WT or mutants) were incubated with indicated substrate in a reaction mixture [50 mM Tris-HCl (pH 7.3), 10 mM magnesium acetate and 0.01% β -mercaptoethanol] together with 100 μ M ³²P[γ -ATP] (0.5 μ Ci/assay) for 15 min. Reactions were stopped by spotting them on p81 paper (Whatman) washed with phosphoric acid and were counted for radioactivity as described previously.³⁹ In assays from cells overexpressing GSK-3 proteins, the activity of the endogenous GSK-3 that was determined in cells transfected with the pCMV4 vector was subtracted from the activity values obtained for WT and mutants.

Statistical analysis

Data were analyzed with Origin Professional 6.0 software using Student's *t*-test to compare GSK-3 activity of WT versus mutants or peptides treatment versus peptides nontreatment. Data were considered significant at $p < 0.05$.

Molecular modeling and dynamics

A model of L803 peptide in helical conformation was built using the Biopolymer module of InsightII (Accelrys Inc., San Diego, CA) and was minimized shortly in water. This preliminary model was used in MD simulations of the free peptide and of the GSK-3 β /ATP-Mg²⁺/L803 complex (GSK-3 β was phosphorylated on Tyr216). In the latter case, the peptide was positioned about 5 Å away from the molecular surface of GSK-3 β with S10(p) opposite the positive phosphate binding cavity, defined by Arg96, Arg180 and Lys205. The same procedure was used to obtain initial models of free PQ9P and of the GSK-3 β /ATP-Mg²⁺/PQ9P complex. The MD simulations were performed using the program Gromacs,⁵³ employing the united atoms gromos96 43a1 force field⁵⁴ modified to include phosphorylated residues[†]. The initial model of the solute (peptide or the GSK-3 β /ATP-Mg²⁺/peptide

[†] http://www.gromacs.org/Downloads/User_contributions/Force_fields

complex) was immersed in a cube of water, neutralized and energy minimized. This was followed by a 1-ns MD simulation to equilibrate the water, keeping the non-hydrogen atoms of the solute restrained. Next, an additional 1-ns or 2-ns simulation of the peptide or the GSK-3 β /ATP-Mg²⁺/peptide complex was performed, respectively, immersed in water. In the latter case, the C α atoms of GSK-3 β were restrained. Only the last 1 ns of each MD simulation was considered in the analysis of the trajectory (0.5 ns for the free peptides). Clustering of conformers from the MD trajectory was executed using the *g_cluster* tool of Gromacs. An ensemble of conformers was obtained by sampling the trajectory at 0.5-ps intervals. Conformers of the free peptides were superposed using all non-hydrogen atoms and were clustered using RMSD values calculated for the same atoms. Conformers of the complexes were superposed using the C α atoms of GSK-3 β and were then clustered using RMSD values calculated for the non-hydrogen atoms of the peptide. The single-linkage method was used for clustering with 1-Å cutoff.

Rigid-body docking

Rigid-body docking was performed with the geometric-electrostatic-hydrophobic version of MolFit,⁴⁸ employing translation and rotation intervals of 1.05 Å and 12°, respectively, as previously described.⁵⁵ The starting geometry of the GSK-3 β /ATP-Mg²⁺ complex, in which Tyr216 is phosphorylated, was modeled as previously described.³⁹ Several conformers of the peptide were docked: central conformers from groups obtained by clustering the MD trajectory of the free peptide in water and additional conformers from the largest MD group selected manually to represent the range of structures within this group. The comprehensive docking scans were followed by a new post-scan filtering procedure that incorporates statistical propensity measures and desolvation energy calculations.⁴⁹ The filtered models were further screened, requesting that S10(p) of the peptide makes contact with the positive cavity on the surface of GSK-3 β . We refer to these models as acceptable models.

Anchoring spots mapping

Anchoring spots mapping identifies preferred binding positions of amino acid side chains on the surface of a protein.⁴¹ This procedure was used here to detect amino acids that bind in the GSK-3 β surface cavity bordered by the loop 89–95 and the P-loop. The cutoff value $\Delta G \leq -4$ kcal/mol was previously found useful for identifying likely hotspot anchors;⁴¹ here, we used a higher cutoff of $\Delta G \leq -3$ kcal/mol to include residues that can bind strongly in the cavity but are not necessarily anchoring hot spots.

Solvent accessibility

Solvent accessibility was calculated with a 1.4-Å probe using the Homology module of InsightII (Accelrys Inc.).

Supplementary materials related to this article can be found online at [doi:10.1016/j.jmb.2011.02.036](https://doi.org/10.1016/j.jmb.2011.02.036)

References

- Manning, G., Plowman, G. D., Hunter, T. & Sudarsanam, S. (2002). Evolution of protein kinase signaling from yeast to man. *Trends Biochem. Sci.* **27**, 514–520.
- Lopez-Otin, C. & Hunter, T. (2010). The regulatory crosstalk between kinases and proteases in cancer. *Nat. Rev., Cancer*, **10**, 278–292.
- Scott, J. D. & Pawson, T. (2009). Cell signaling in space and time: where proteins come together and when they're apart. *Science*, **326**, 1220–1224.
- Taylor, S. S., Knighton, D. R., Zheng, J., Sowadski, J. M., Gibbs, C. S. & Zoller, M. J. (1993). A template for the protein kinase family. *Trends Biochem. Sci.* **18**, 84–89.
- Hunter, T. (2009). Tyrosine phosphorylation: thirty years and counting. *Curr. Opin. Cell Biol.* **21**, 140–146.
- Knight, Z. A., Lin, H. & Shokat, K. M. (2010). Targeting the cancer kinome through polypharmacology. *Nat. Rev., Cancer*, **10**, 130–137.
- Cohen, P. (2002). Protein kinases—the major drug targets of the twenty-first century? *Nat. Rev., Drug Discov.* **1**, 309–315.
- Blume-Jensen, P. & Hunter, T. (2001). Oncogenic kinase signalling. *Nature*, **411**, 355–365.
- Lemmon, M. A. & Schlessinger, J. (2010). Cell signaling by receptor tyrosine kinases. *Cell*, **141**, 1117–1134.
- Davies, S. P., Reddy, H., Caivano, M. & Cohen, P. (2000). Specificity and mechanism of action of some commonly used protein kinase inhibitors. *Biochem. J.* **351**, 95–105.
- Eldar-Finkelman, H. & Eisenstein, M. (2009). Peptide inhibitors targeting protein kinases. *Curr. Pharm. Des.* **15**, 2463–2470.
- Frame, S. & Cohen, P. (2001). GSK-3 takes center stage more than 20 years after its discovery. *Biochem. J.* **359**, 1–16.
- Doble, B. W. & Woodgett, J. R. (2003). GSK-3: tricks of the trade for a multi-tasking kinase. *J. Cell Sci.* **116**, 1175–1186.
- Grimes, C. A. & Jope, R. S. (2001). The multifaceted roles of glycogen synthase kinase 3 β in cellular signaling. *Prog. Neurobiol.* **65**, 391–426.
- Hur, E. M. & Zhou, F. Q. (2010). GSK3 signalling in neural development. *Nat. Rev., Neurosci.* **11**, 539–551.
- Kim, W. Y., Wang, X., Wu, Y., Doble, B. W., Patel, S., Woodgett, J. R. & Snider, W. D. (2009). GSK-3 is a master regulator of neural progenitor homeostasis. *Nat. Neurosci.* **12**, 1390–1397.
- Eldar-Finkelman, H. (2002). Glycogen synthase kinase-3: an emerging therapeutic target. *Trends Mol. Med.* **8**, 126–132.
- Jope, R. S., Yuskaitis, C. J. & Beurel, E. (2007). Glycogen synthase kinase-3 (GSK3): inflammation, diseases, and therapeutics. *Neurochem. Res.* **32**, 577–595.
- O'Brien, W. T. & Klein, P. S. (2009). Validating GSK3 as an *in vivo* target of lithium action. *Biochem. Soc. Trans.* **37**, 1133–1138.
- Gould, T. D., Zarate, C. A. & Manji, H. K. (2004). Glycogen synthase kinase-3: a target for novel bipolar disorder treatments. *J. Clin. Psychiatry*, **65**, 10–21.

21. Lovestone, S., Killick, R., Di Forti, M. & Murray, R. (2007). Schizophrenia as a GSK-3 dysregulation disorder. *Trends Neurosci.* **30**, 142–149.
22. Bhat, R. V., Budd Haerberlein, S. L. & Avila, J. (2004). Glycogen synthase kinase 3: a drug target for CNS therapies. *J. Neurochem.* **89**, 1313–1317.
23. Cohen, P. & Goedert, M. (2004). GSK3 inhibitors: development and therapeutic potential. *Nat. Rev., Drug Discov.* **3**, 479–487.
24. Meijer, L., Flajolet, M. & Greengard, P. (2004). Pharmacological inhibitors of glycogen synthase kinase 3. *Trends Pharmacol. Sci.* **25**, 471–480.
25. Eldar-Finkelman, H., Licht-Murava, A., Pietrovski, S. & Eisenstein, M. (2010). Substrate competitive GSK-3 inhibitors—strategy and implications. *Biochim. Biophys. Acta*, **1804**, 598–603.
26. Martinez, A. & Perez, D. I. (2008). GSK-3 inhibitors: a ray of hope for the treatment of Alzheimer's disease? *J. Alzheimer's Dis.* **15**, 181–191.
27. Plotkin, B., Kaidanovich, O., Talior, I. & Eldar-Finkelman, H. (2003). Insulin mimetic action of synthetic phosphorylated peptide inhibitors of glycogen synthase kinase-3. *J. Pharmacol. Exp. Ther.* **305**, 974–980.
28. Woodgett, J. R. & Cohen, P. (1984). Multisite phosphorylation of glycogen synthase. Molecular basis for the substrate specificity of glycogen synthase kinase-3 and casein kinase-II (glycogen synthase kinase-5). *Biochim. Biophys. Acta*, **788**, 339–347.
29. Fiol, C. J., Mahrenholz, A. M., Wang, Y., Roeske, R. W. & Roach, P. J. (1987). Formation of protein kinase recognition sites by covalent modification of the substrate. Molecular mechanism for the synergistic action of casein kinase II and glycogen synthase kinase 3. *J. Biol. Chem.* **262**, 14042–14048.
30. Dajani, R., Fraser, E., Roe, S. M., Young, N., Good, V., Dale, T. C. & Pearl, L. H. (2001). Crystal structure of glycogen synthase kinase 3 β : structural basis for phosphate-primed substrate specificity and autoinhibition. *Cell*, **105**, 721–732.
31. ter Haar, E., Coll, J. T., Austen, D. A., Hsiao, H. M., Swenson, L. & Jain, J. (2001). Structure of GSK3 β reveals a primed phosphorylation mechanism. *Nat. Struct. Biol.* **8**, 593–596.
32. Chu, B., Soncin, F., Price, B. D., Stevenson, M. A. & Calderwood, S. K. (1996). Sequential phosphorylation by mitogen-activated protein kinase and glycogen synthase kinase 3 represses transcriptional activation by heat shock factor-1. *J. Biol. Chem.* **271**, 30847–30857.
33. Kaidanovich-Beilin, O. & Eldar-Finkelman, H. (2005). Long-term treatment with novel glycogen synthase kinase-3 inhibitor improves glucose homeostasis in ob/ob mice: molecular characterization in liver and muscle. *J. Pharmacol. Exp. Ther.* **316**, 17–24.
34. Rao, R., Hao, C. M., Redha, R., Wasserman, D. H., McGuinness, O. P. & Breyer, M. D. (2007). Glycogen synthase kinase 3 inhibition improves insulin-stimulated glucose metabolism but not hypertension in high-fat-fed C57BL/6J mice. *Diabetologia*, **50**, 452–460.
35. Kim, W. Y., Zhou, F. Q., Zhou, J., Yokota, Y., Wang, Y. M., Yoshimura, T. *et al.* (2006). Essential roles for GSK-3s and GSK-3-primed substrates in neurotrophin-induced and hippocampal axon growth. *Neuron*, **52**, 981–996.
36. Chen, G., Bower, K. A., Ma, C., Fang, S., Thiele, C. J. & Luo, J. (2004). Glycogen synthase kinase 3 β (GSK3 β) mediates 6-hydroxydopamine-induced neuronal death. *FASEB J.* **18**, 1162–1164.
37. Kaidanovich-Beilin, O., Milman, A., Weizman, A., Pick, C. & Eldar-Finkelman, H. (2004). Rapid antidepressive like activity of specific GSK-3 inhibitor, and its effect on -catenin in the mouse hippocampus. *Biol. Psychiatry*, **55**, 781–784.
38. Shapira, M., Licht, A., Milman, A., Pick, C. G., Shohami, E. & Eldar-Finkelman, H. (2007). Role of glycogen synthase kinase-3 β in early depressive behavior induced by mild traumatic brain injury. *Mol. Cell. Neurosci.* **34**, 571–577.
39. Ilouz, R., Kowelsman, N., Eisenstein, M. & Eldar-Finkelman, H. (2006). Identification of novel glycogen synthase kinase-3 β substrate-interacting residues suggests a common mechanism for substrate recognition. *J. Biol. Chem.* **281**, 30621–30630.
40. Bertrand, J. A., Thieffine, S., Vulpetti, A., Cristiani, C., Valsasina, B., Knapp, S. *et al.* (2003). Structural characterization of the GSK-3 β active site using selective and non-selective ATP-mimetic inhibitors. *J. Mol. Biol.* **333**, 393–407.
41. Ben-Shimon, A. & Eisenstein, M. (2010). Computational mapping of anchoring spots on protein surfaces. *J. Mol. Biol.* **402**, 259–277.
42. Cole, A., Frame, S. & Cohen, P. (2004). Further evidence that the tyrosine phosphorylation of glycogen synthase kinase-3 (GSK3) in mammalian cells is an autophosphorylation event. *Biochem. J.* **377**, 249–255.
43. Eldar-Finkelman, H., Agrast, G. M., Foord, O., Fischer, E. H. & Krebs, E. G. (1996). Expression and characterization of GSK-3 mutants and their effect on glycogen synthase activity. *Proc. Natl Acad. Sci. USA*, **93**, 10228–10233.
44. Liberman, Z. & Eldar-Finkelman, H. (2005). Serine 332 phosphorylation of insulin receptor substrate-1 by glycogen synthase kinase-3 attenuates insulin signaling. *J. Biol. Chem.* **280**, 4422–4428.
45. Fiol, C. J., Williams, J. S., Chou, C. H., Wang, Q. M., Roach, P. J. & Andrisani, O. M. (1994). A secondary phosphorylation of CREB341 at Ser129 is required for the cAMP-mediated control of gene expression. A role for glycogen synthase kinase-3 in the control of gene expression. *J. Biol. Chem.* **269**, 32187–32193.
46. Liberman, Z., Plotkin, B., Tennenbaum, T. & Eldar-Finkelman, H. (2008). Coordinated phosphorylation of insulin receptor substrate-1 by glycogen synthase kinase-3 and protein kinase C β II in the diabetic fat tissue. *Am. J. Physiol.: Endocrinol. Metab.* **294**, E1169–E1177.
47. Ojo, K. K., Gillespie, J. R., Riechers, A. J., Napuli, A. J., Verlinde, C. L., Buckner, F. S. *et al.* (2008). Glycogen synthase kinase 3 is a potential drug target for African trypanosomiasis therapy. *Antimicrob. Agents Chemother.* **52**, 3710–3717.
48. Berchanski, A., Shapira, B. & Eisenstein, M. (2004). Hydrophobic complementarity in protein-protein docking. *Proteins*, **351**, 309–326.
49. Kowalsman, N. & Eisenstein, M. (2009). Combining interface core and whole interface descriptors in

- postscan processing of protein-protein docking models. *Proteins*, **77**, 297–318.
50. Heifetz, A. & Eisenstein, M. (2003). Effect of local shape modifications of molecular surfaces on rigid-body protein-protein docking. *Protein Eng.* **16**, 179–185.
 51. Ben-Zeev, E. & Eisenstein, M. (2003). Weighted geometric docking: incorporating external information in the rotation-translation scan. *Proteins*, **52**, 24–27.
 52. Hughes, K., Nicolakaki, E., Plyte, S. E., Totty, N. F. & Woodgett, J. R. (1993). Modulation of glycogen synthase kinase-3 family by tyrosine kinase phosphorylation. *EMBO J.* **12**, 803–808.
 53. Van Der Spoel, D., Lindahl, E., Hess, B., Groenhof, G., Mark, A. E. & Berendsen, H. J. (2005). GROMACS: fast, flexible, and free. *J. Comput. Chem.* **26**, 1701–1718.
 54. Lindhal, E., Hess, B. & van der Spoel, D. (2001). GROMACS 3.0: a package for molecular simulation and trajectory analysis. *J. Mol. Model.* **7**, 306–317.
 55. Kowalsman, N. & Eisenstein, M. (2007). Inherent limitations in protein-protein docking procedures. *Bioinformatics*, **23**, 421–426.